Inorg. Chem. **2004**, *43*, 3573–3581

A Detailed Study of the Vapochromic Behavior of $\{Tl[Au(C_6Cl_5)_2]\}_n$

Eduardo J. Fernández, José M. López-de-Luzuriaga, Miguel Monge, Manuel Montiel, M. Elena Olmos, and Javier Pérez

Grupo de Síntesis Química de La Rioja, Departamento de Química, Universidad de La Rioja, UA-CSIC, Madre de Dios 51, E-26004 Logroño, Spain

Antonio Laguna*

Departamento de Química Inorgánica-ICMA, Universidad de Zaragoza-CSIC, E-50009 Zaragoza, Spain

Fernando Mendizabal

Departamento de Química, Facultad de Ciencias, Universidad de Chile, Casilla 653-Santiago, Chile

Ahmed A. Mohamed and John P. Fackler, Jr.*

Department of Chemistry and Laboratory for Molecular Structure and Bonding, Texas A&M University, P.O. Box 30012 College Station, Texas 77842-3012

Received January 13, 2004

The linear-chain polymer $\{Tl[Au(C_6Cl_5)_2]\}_n$, **1**, reacts in the solid state and in solution with different volatile organic compounds such as tetrahydrofuran, acetone, tetrahydrothiophene, 2-fluoropyridine, acetonitrile, acetylacetone, and pyridine. Solid-state exposure of **1** to vapors of the above VOCs produces a selective and reversible change in its color that is perceptible to the human eye and even deeper under UV irradiation, allowing **1** to function as a sensor for these VOCs. Heating the samples exposed to the VOCs for a few minutes at 100° C regenerates the original material without degradation, even after several exposure/heating cycles. The reversibility is further confirmed by X-ray powder diffraction measurements of complex **1** before and after exposure to vapors and again after heating the samples. The products obtained by reactions of complex **1** with the above VOCs as ligands in solution contain extended linear chains of alternating gold and thallium centers with two molecules of the organic ligands attached to each thallium atom. The stoichiometry of these materials has been confirmed by single-crystal X-ray diffraction as $\{Tl(THF)_2[Au(C_6Cl_5)_2]\}_n$, **3**, and $\{Tl(acacH)_2[Au(C_6Cl_5)_2]\}_n$, **5**. Comparison of FT-IR, UV–vis, and luminescence spectra at room temperature and at 77 K of the solid samples of complexes **2**–**9** with the spectra of complex **1** after its exposure to VOCs suggests interaction occurs between the organic VOCs and thallium in each case. Thermogravimetric analyses data indicate that all the thallium centers in these derivatives of complex **1** are neither fully nor equally coordinatively saturated. The materials formed appear to be intermediates between complex **1** with no VOCs attached and complexes **3**–**9** which contain two organic ligands coordinated to each thallium. A crystal structure analyses of one of these intermediates, $\{Tl(THF)_{0.5}[Au(C_6Cl_5)_2]\}_n$, **1**·0.5THF, confirms this. Density functional calculations are in accord with the observed experimental results. Analysis reveals a substantial participation of the metal atoms in transitions that give rise to the observed emissions. Crystallographic data are as follows. For **1**·0.5THF: triclinic, $P\bar{1}$, $a = 8.9296(1)$ Å, $b = 11.2457(1)$ Å, $c = 21.2465(3)$ Å, $\alpha = 96.7187(7)°$, $\beta = 92.5886(6)°$, $\gamma = 98.5911(8)°$, $V = 2090.87(4)$ Å^3, and $Z = 2$. For **3**: monoclinic, $P2_1/c$, $a = 26.4163(6)$ Å, $b = 12.1619(2)$ Å, $c = 28.0813(6)$ Å, $\alpha = 90°$, $\beta = 161.9823(6)°$, $\gamma = 90°$, $V = 2790.51(10)$ Å^3, and $Z = 4$. For **5**: monoclinic, $P2_1/c$, $a = 9.8654(2)$ Å, $b = 29.8570(5)$ Å, $c = 11.6067(2)$ Å, $\alpha = 90°$, $\beta = 114.5931(6)°$, $\gamma = 90°$, $V = 3108.64(10)$ Å^3, and $Z = 4$.

Introduction

Reversible and highly stable chemical sensor materials have received increased attention in the past few years, and, among the many types of sensors, vapochromic or vapoluminescent compounds are of special interest. Indeed, materials that show a unique response to volatile organic compounds (VOCs), especially those displaying appreciable selectivity at low VOC levels with dramatic changes of color or emission, are of considerable importance.[1−5] In this sense,

* Authors to whom correspondence should be addressed. E-mail: fackler@mail.chem.tamu.edu; alaguna@posta.unizar.es.

10.1021/ic0499446 CCC: $27.50
Published on Web 05/15/2004

some polymeric molecular compounds (based on weak intermolecular interactions) show important changes in their optical properties in the presence of solvents. For example, "double salts" of the type $[Pt(CNR)_4][Pt(CN)_4]$ reported by Mann and co-workers,[1a] change their absorption and emission spectra upon exposure to vapors of various solvents. Balch's[6] solvoluminescent $[Au_3(CH_3N{=}COCH_3)_3]$ and Eisenberg's[2] $[AuS_2CN(C_5H_{11})_2]_2$ are interesting examples of gold(I) compounds which show unusual luminescence behavior in the presence of some organic solvents.

Polymeric materials such as the heterobimetallic d^{10}-s^2 Au(I)···Tl(I) systems are of special interest, not only for their structural versatility which includes infinite linear chains[7−10] with 2D or 3D networks,[11] polynuclear complexes,[12] metallocryptates,[13] or discrete molecules,[14] but also for their photophysical properties.[7−14] Recently we have focused our attention on the use of the acid−base stacking phenomenon for the formation of polymeric, intermetallic Au(I)···Tl(I) complexes. For this purpose, $[AuR_2]^-$ ($R = C_6F_5^-$, $C_6Cl_5^-$), a Lewis base, has been reacted with $TlPF_6$, wherein Tl(I) functions a Lewis acid, in the presence[8,10,11] or even in the absence[9] of stabilizing ligands. These reactions generally give rise to extended unsupported Au(I)···Tl(I) polymeric chains in which the most important structural motif for the existence of polynuclear or polymeric frameworks is the Au(I)···Tl(I) interaction. We have carried out theoretical studies which show that the Au(I)···Tl(I) interaction has a stabilizing energy of about 275 kJ/mol. The ionic contribution to this energy is the most important (80%) while van der Waals dispersion interactions also are significant (20%). Moreover, time-dependent density functional theory (TDDFT) calculations of several $Au(I)R_2-Tl(I)L_n$ systems show that the geometrical environment around the Tl(I) centers and the Au−Tl distances are important contributors to interpretations of the optical properties of these systems.[10]

Recently some of us have communicated results involving Au(I)···Tl(I) interactions in extended unsupported Au(I)···Tl(I) linear chains without stabilizing ligands at Tl(I) centers, $\{Tl[Au(C_6Cl_5)_2]\}_n$.[9] A very interesting feature of this material is its vapochromic behavior with a variety of VOCs. Indeed, the 3D Au(I)···Tl(I) network of this compound displays channels parallel to the *z* axis, with diameters as large as 10.471 Å, which allow solvent molecules to enter the lattice. These solvents interact with the Tl(I) centers to produce changes in the optical properties and stability of the Au(I)···Tl(I) chains.

This paper reports details of the vapochromic behavior and other properties of $\{Tl[Au(C_6Cl_5)_2]\}_n$, **1**, using thermogravimetric analysis (TGA), powder and/or single-crystal X-ray diffraction, FT-IR, UV−vis absorption, and luminescence measurements. Moreover, we describe the syntheses and characterization of the new extended linear chain Au(I)···Tl(I) complexes $\{TlL_2[Au(C_6Cl_5)_2]\}_n$ (L = THF, **3**; THT, **4**; acacH, **5**; 2-fluoropyridine, **6**; NEt_3, **7**; py, **8**; NCMe, **9**), which form upon solution reactions of the ligands with $\{Tl[Au(C_6Cl_5)_2]\}_n$. Finally, we discuss the theoretical calculations used to help understand the photophysical properties of this system.

Experimental Section

Experimental. All the volatile organic compounds were purchased from Aldrich and used as received. The complex $\{Tl[Au(C_6Cl_5)_2]\}_n$ was prepared as described previously.[9]

Instrumentation. Infrared spectra were recorded in the 4000−200 cm^{-1} range using a Perkin-Elmer FT-IR Spectrum 1000 spectrophotometer in Nujol mulls between polyethylene sheets. C, H, and N analyses were carried out with a C. E. Instrument EA-1110 CHNS−O microanalyzer. Mass spectra were recorded on a HP-5989B API-Electrospray Mass Spectrometer with interface 59987A. ^1H and ^{19}F NMR spectra were recorded on a Bruker ARX 300 in $(CD_3)_2CO$, d_8−THF and d_6-benzene solutions. Chemical shifts are reported relative to $SiMe_4$ (^1H external) and $CFCl_3$ (^{19}F external). Excitation and emission spectra were recorded on a Jobin-Yvon Horiba Fluorolog 3-22 Tau-3 spectrofluorimeter. Acetone used in the photophysical studies was distilled over potassium permanganate and degassed before use. Fluorescence lifetime measurements were recorded operating in the phase-modulation mode. The phase shift and modulation were recorded over the frequency range 0.1−50 MHz and data were fitted using the Jobin-Yvon software package. Thermogravimetric analyses (TGA) were recorded on a TA Instruments SDT 2960 using 5−10 mg samples.

Preparation of the Complexes $\{TlL_2[Au(C_6Cl_5)_2]\}_n$ (L = THF, 3; THT, 4; acacH, 5; 2-fluoropyridine, 6; NEt_3, 7; py, 8; NCMe, 9). To a suspension of $[AuTl(C_6Cl_5)_2]_n$[9] (100 mg, 0.111 mmol) in toluene (35 mL) was added THT (19 mg, 0.222 mmol), **4**; acacH (22.2 mg, 0.222 mmol), **5**; 2-fluoropyridine (21.6 mg, 0.222 mmol), **6**; NEt_3 (22.4 mg, 0.222 mmol), **7**; py (17.6 mg, 0.222 mmol), **8**. Complexes **3** and **9** were obtained using THF or NCMe, respectively, utilizing the lower ability of these solvents to coordinate as ligands. The solutions were stirred for 50 min followed by evaporation of the solvents in a vacuum. The resulting solids were washed with *n*-hexane (20 mL) and isolated by filtration (yields ∼75%).

Complexes **3**−**8** show different colors: green for **3**, different yellow intensities for **4**, **6**, **7**, and **9**, red for **5**, and deep red for **8**.

(1) (a) Buss, C. E.; Mann, K. R. *J. Am. Chem. Soc.* **2002**, *124*, 1031. (b) Dias, H. V.; Diyabalalage, H. V.; Rawashdeh-Omary, M.; Franzman, M. A.; Omary, M. A. *J. Am. Chem. Soc.* **2003**, *125*, 12072.
(2) Mansour, M. A.; Connick, W. B.; Lachicotte, R. J.; Gysling, H. J.; Eisenberg, R. *J. Am. Chem. Soc.* **1998**, *120*, 1329.
(3) Beauvais, L. G.; Shores, M. P.; Long, J. R. *J. Am. Chem. Soc.* **2000**, *122*, 2763.
(4) Cariati, E.; Bu, X.; Ford, P. C. *Chem. Mater.* **2000**, *12*, 3385.
(5) Evju, J. K.; Mann, K. R. *Chem. Mater.* **1999**, *11*, 1425.
(6) Vickery, J. C.; Olmstead, M. M.; Fung, E. Y.; Balch, A. L. *Angew. Chem., Int. Ed. Engl.* **1997**, *36*, 1179.
(7) (a) Wang, S.; Fackler, J. P., Jr.; King, C.; Wang, J. C. *J. Am. Chem. Soc.* **1988**, *110*, 3308. (b) Wang, S.; Garzón, G.; King, C.; Wang, J. C.; Fackler, J. P., Jr. *Inorg. Chem.* **1989**, *28*, 4623.
(8) Crespo, O.; Fernández, E. J.; Jones, P. G.; Laguna, A.; López-de-Luzuriaga, J. M.; Mendía, A.; Monge, M.; Olmos, E. *Chem. Commun.* **1998**, 2233.
(9) Fernández, E. J.; López-de-Luzuriaga, J. M.; Monge, M.; Olmos, E.; Pérez, J.; Laguna, A.; Mohamed, A. A.; Fackler, J. P., Jr. *J. Am. Chem. Soc.* **2003**, *125*, 2022.
(10) Fernández, E. J.; Laguna, A.; López-de-Luzuriaga, J. M.; Mendizábal, F.; Monge, M.; Olmos, E.; Pérez, J. *Chem. Eur. J.* **2003**, *9*, 456.
(11) Fernández, E. J.; Jones, P. G.; Laguna, A.; López-de-Luzuriaga, J. M.; Monge, M.; Olmos, E.; Pérez, J. *Inorg. Chem.* **2002**, *41*, 1056.
(12) Burini, A.; Bravi, R.; Fackler, J. P., Jr.; Galassi, R.; Grant, T. A.; Omary, M. A.; Pietroni, B. R.; Staples, R. J. *Inorg. Chem.* **2000**, *39*, 3158.
(13) Catalano, V. J.; Bennett, B. L.; Kar, H. M.; Noll, B. C. *J. Am. Chem. Soc.* **1999**, *121*, 10235.
(14) Fernández, E. J.; López-de-Luzuriaga, J. M.; Monge, M.; Olmos, E.; Pérez, J.; Laguna, A. *J. Am. Chem. Soc.* **2002**, *124*, 5942.

Crystals of **3** and **5** suitable for X-ray diffraction were obtained by slow diffusion of *n*-hexane into a concentrated toluene solution of the complexes. Elemental analysis calcd (%) for **3** ($C_{20}H_{16}AuCl_{10}O_2Tl$): C, 23.00; H, 1.54. Found: C, 23.10; H, 1.47. Calcd for **4** ($C_{20}H_{16}AuCl_{10}S_2Tl$): C, 22.32; H, 1.50; S, 5.96. Found: C, 22.0; H, 1.45; S, 6.3. Calcd for **5** ($C_{22}H_{16}AuCl_{10}O_4Tl$): C, 24.02; H, 1.47. Found: C, 23.90; H, 1.48. Calcd for **6** ($C_{22}H_8AuCl_{10}F_2N_2Tl$): C, 24.15; H, 0.74; N, 2.56. Found: C, 23.91; H, 0.57; N, 2.90. Calcd for **7** ($C_{24}H_{30}AuCl_{10}N_2Tl$): C, 26.15; H, 2.74; N, 2.54. Found: C, 26.02; H, 2.66; N, 2.29. Calcd for **8** ($C_{22}H_{10}AuCl_{10}N_2Tl$): C, 24.97; H, 0.95; N, 2.65. Found: C, 25.15; H, 0.71; N 2.57. Calcd for **9** ($C_{16}H_6AuCl_{10}N_2Tl$): C, 19.57; H, 0.62; N, 2.85. Found: C, 20.00; H, 0.82; N, 3.15. ^{1}H NMR: **3** (298 K, $(CD_3)_2CO$) δ 1.79 (m, 4H, CH_2), δ 3.62 (m, 4H, CH_2). ^{1}H NMR: **4** (298 K, (d_6−benzene) δ 1.44 (m, 4H, CH_2), δ 2.54 (m, 4H, CH_2). ^{1}H NMR: **5** (298 K, d_8−THF) δ 2.19 (s, 6H, CH_3), δ 3.56 (s, 2H, CH_2), δ 1.99 (s, 6H, CH_3), δ 5.56 (s, H, CH). ^{19}F NMR (298 K, d_8−THF): **6** δ −137.9 (m, 2-fluoropyridine). ^{1}H NMR (298 K, d_8-THF): **6** 8.17−6.96 ppm (m, H-aromatic). ^{1}H NMR (298 K, d_8−THF): **7** δ 2.42 (c, 6H, CH_2 J_{H-H}= 5.5 Hz), δ 1.01 (t, 9H, CH_3 J_{H-H}= 5.5 Hz). ^{1}H NMR (298 K, d_8−THF): **8** δ 8.52−6.67 ppm (m, H-aromatic). ^{1}H NMR (298 K, d_8−THF): **9** δ 1.95 (s, CH_3). Mass spectra for **3**−**9** (ES−) m/z = 695 (100%), $[Au(C_6Cl_5)_2]^-$ and (ES+) m/z = 204 (100%), Tl^+.

Crystallography. Crystals of **3**, **5**, and **1**·0.5THF were mounted in inert oil on glass fibers and transferred to the cold gas stream of a Nonius Kappa CCD diffractometer equipped with an Oxford Instruments low-temperature attachment. Data were collected using monochromated Mo Kα radiation (λ = 0.71073 Å). Absorption corrections were made numerically based on multiple scans. The structures were solved by direct methods and refined on F^2 using the program SHELXL-97.[15] All nonhydrogen atoms were refined anisotropically. Hydrogen atoms were included using a riding model for **3**, or mixed models for **5** and **1**·0.5THF. Further details of the data collection and refinement are given in Table 1. Selected bond lengths and angles are presented in Table 2, and the crystal structures of **3**, **5**, and **1**·0.5THF are shown in Figures 2−7 in the Results. Room temperature (23 °C) X-ray powder diffraction patterns were obtained using a D-Max Rigaku System with 80 mA and 40 kV sealed copper source equipped with a single-crystal graphite monochromator and scintillation counter. Powder diffraction patterns were collected between 2θ of 5° and 70° with a 2θ stepping angle of 0.03° and an angle dwell of 1 s. Where appropriate, powder patterns also were calculated from the observed single-crystal data.

Computational Methods. In DFT and TDDFT calculations, the molecular structure used in the theoretical studies of $Tl[Au(C_6Cl_5)_2]_2$, **1a**, the dimer portion of the polymer, was taken from the X-ray structure of **1**. All distances and angles were kept constant in the single-point DFT calculations. In both the single-point ground-state calculations and the subsequent calculations of the electronic excitation spectra, the default Becke−Perdew (B−P) functional,[16−18] as implemented in TURBOMOLE,[19] was used. The excitation energies were obtained at the density functional level using the time-dependent perturbation theory approach (TDDFT),[20−24] which is a density-functional-theory generalization of the Hartree−Fock linear response (HFLR) or random phase approximation (RPA) method.[25] In all calculations, the Karlsruhe split-valence quality basis sets,[26] augmented with polarization functions,[27] were used (SVP). The Stuttgart effective core potentials in TURBOMOLE were used for Au and Tl.[28] Calculations were performed without assuming C_2 symmetry in **1a**.

Table 1. Details of X-ray Data Collection and Structure Refinement for Complexes **3**, **5**, and **1**·0.5 THF

compound	**3**	**5**	**1**·0.5 THF
chemical formula	$C_{20}H_{16}AuCl_{10}O_2Tl$	$C_{22}H_{16}AuCl_{10}O_4Tl$	$C_{28}H_8Au_2Cl_{20}OTl_2$
cryst habit	yellow plate	red prism	yellow plate
cryst size/mm	0.20 × 0.18 × 0.08	0.50 × 0.1 × 0.07	0.20 × 0.20 × 0.08
cryst syst	monoclinic	monoclinic	triclinic
space group	$P2_1/c$	$P2_1/c$	$P\bar{1}$
a (Å)	26.4163(6)	9.8654(2)	8.9296(1)
b (Å)	12.1619(2)	29.8570(5)	11.2457(1)
c (Å)	28.0813(6)	11.6067(2)	21.2465(3)
α (°)	90	90	96.7187(7)
β (°)	161.9823(6)	114.5931(6)	92.5886(6)
γ (°)	90	90	98.5911(8)
U (Å^3)	2790.51(10)	3108.64(10)	2090.87(4)
Z	4	4	2
D_c (g cm^{-3})	2.485	2.351	2.973
M	1044.16	1100.18	1872.02
F(000)	1928	2040	1688
T (°C)	−100	25	−100
$2\theta_{max}$ (°)	56	56	56
μ(Mo Kα) (mm^{-1})	11.996	10.779	15.986
No. of reflns collected	19014	7252	30489
No. of unique reflns	6610	4849	9932
R_{int}	0.058	0.064	0.052
R^a (I>2σ(I))	0.0457	0.0485	0.0346
wR^b (F^2, all refl.)	0.0934	0.1256	0.0850
No. of parameters	307	349	479
No. of restraints	84	90	138
S^c	1.016	1.052	1.039
max. $\Delta\rho$ (eÅ^{-3})	1.682	2.240	1.819

[a] $R(F) = \sum||F_o| - |F_c||/\sum|F_o|$. [b] $wR(F^2) = |\sum\{w(F_o^2 - F_c^2)^2\}/\sum\{w(F_o^2)^2\}]^{0.5}$; $w^{-1} = \sigma^2(F_o^2) + (aP)^2 + bP$, where $P = [F_o^2 + 2F_c^2]/3$ and a and b are constants adjusted by the program. [c] $S = [\sum\{w(F_o^2 - F_c^2)^2\}/(n - p)]^{0.5}$, where n is the number of data and p is the number of parameters.

Results and Discussion

Synthesis. The linear-chain polymer $\{Tl[Au(C_6Cl_5)_2]\}_n$, **1**, was obtained by reacting $Bu_4N[Au(C_6Cl_5)_2]$ with the Lewis acid Tl(1+), as the hexafluorophosphate salt, in equimolecular amounts in tetrahydrofuran.[9] Complex **1** was reacted in THF or in the pure organic ligands as solvents in a 1:2 molar ratio. All the complexes obtained from these solutions show the same stoichiometry $\{TlL_2[Au(C_6Cl_5)_2]\}_n$ (L = THF, **3**; THT, **4**; acacH, **5**; 2-fluoropyridine, **6**; NEt_3, **7**; py, **8**; NCMe, **9**), except in the case of acetone which produced the molecular complex $[Au_2Tl_2(C_6Cl_5)_4]\cdot(CH_3)_2C{=}O$, **2**. This material has been previously reported by some of us[14] and

(15) Sheldrick, G. M. *SHELXL-97, A Program for Crystal Structure Refinement*; University of Göttingen: Göttingen, Germany, 1997.
(16) Vosko, S. H.; Wilk, L.; Nusair, M. *Can. J. Phys.* **1980**, *58*, 1200.
(17) Perdew, J. P. *Phys. Rev. B* **1986**, *33*, 8822.
(18) Becke, A. D. *Phys. Rev. B* **1988**, *38*, 3098.
(19) Ahlrichs, R.; Bär, M.; Häser, M.; Horn, H.; Kölmel, C. *Chem. Phys. Lett.* **1989**, *162*, 165.
(20) Bauernschmitt, R.; Ahlrichs, R. *Chem. Phys. Lett.* **1996**, *256*, 454.
(21) Bauernschmitt, R.; Ahlrichs, R. *J. Chem. Phys.* **1996**, *104*, 9047.
(22) Bauernschmitt, R.; Häser, M.; Treutler, O.; Ahlrichs, R. *Chem. Phys. Lett.* **1997**, *264*, 573 and references cited therein.
(23) Gross, E. K. U.; Kohn, W. *Adv. Quantum Chem.* **1990**, *21*, 255.
(24) Casida, M. E. In *Recent Advances in Density Functional Methods, Vol. 1*; Chong, D. P., Ed.; World Scientific: River Edge, NJ, 1995.
(25) Olsen, J.; Jørgensen, P. In *Modern Electronic Structure Theory, Vol. 2*; Yarkony, D. R., Ed.; World Scientific: River Edge, NJ, 1995.
(26) Schäfer, A.; Horn, H.; Ahlrichs, R. *J. Chem. Phys.* **1992**, *97*, 2571.
(27) Dunning, T. H., Jr. *J. Chem. Phys.* **1994**, *100*, 5829.
(28) Andrae, D.; Haeussermann, U.; Dolg, M.; Stoll, H.; Preuss, H. *Theor. Chim. Acta* **1990**, *77*, 123.

Table 2. Selected Bond Lengths [Å] and Angles [deg] for **3**, **5**, and **1**·0.5 THF

	Complex **3**[a]		
Au−Tl#1	3.0764(4)	Au−Tl	3.1981(4)
Au−C(11)	2.071(8)	Au−C(1)	2.082(8)
Tl−O(2)	2.648(6)	Tl−O(1)	2.653(7)
C(11)−Au−C(1)	179.7(2)	Tl#1−Au−Tl	156.506(11)
Au#2−Tl−Au	164.084(12)	O(1)−Tl−Au	109.41(15)
O(2)−Tl−O(1)	78.8(2)	O(2)−Tl−Au#2	99.88(12)
O(1)−Tl−Au#2	86.26(15)	O(2)−Tl−Au	86.33(13)
	Complex **5**[b]		
Au−C(11)	2.063(10)	Au−C(1)	2.069(9)
Au−Tl	2.9684(5)	Au−Tl#1	2.9894(5)
Tl−O(31)	2.626(8)	Tl−O(21)	2.692(9)
O(21)−C(23)	1.261(13)	O(22)−C(24)	1.312(15)
O(31)−C(33)	1.267(13)	O(32)−C(34)	1.313(15)
C(11)−Au−C(1)	178.4(3)	Tl−Au−Tl#1	170.018(18)
Au−Tl−Au#2	155.097(16)	O(21)−Tl−Au#2	115.6(2)
O(31)−Tl−O(21)	74.1(3)	O(31)−Tl−Au	106.72(19)
O(21)−Tl−Au	87.9(2)	O(31)−Tl−Au#2	88.6(2)
C(23)−O(21)−Tl	125.0(8)		
	1·0.5 THF[c]		
Au(1)−C(11)	2.057(6)	Au(1)−C(1)	2.065(6)
Au(2)−C(21)	2.058(6)	Au(2)−C(31)	2.060(6)
Au(1)−Tl(1)#1	2.9078(3)	Au(1)−Tl(2)	3.0918(3)
Au(2)−Tl(1)	2.9794(3)	Au(2)−Tl(2)	3.0267(3)
Tl(2)−O	2.697(6)		
C(11)−Au(1)−C(1)	176.0(2)	Tl(1)#1−Au(1)−Tl(2)	130.142(10)
C(21)−Au(2)−C(31)	179.0(2)	Tl(1)−Au(2)−Tl(2)	175.570(11)
Au(1)#2−Tl(1)−Au(2)	138.712(11)	Au(2)−Tl(2)−Au(1)	157.060(11)
O−Tl(2)−Au(1)	107.69(14)	O−Tl(2)−Au(2)	92.16(14)

[a] Symmetry transformations used to generate equivalent atoms: #1 $-x$, $y + 1/2$, $-z + 1/2$; #2 $-x$, $y - 1/2$, $-z + 1/2$. [b] Symmetry transformations used to generate equivalent atoms: #1 x, $-y + 1/2$, $z + 1/2$; #2 x, $-y + 1/2$, $z - 1/2$. [c] Symmetry transformations used to generate equivalent atoms: #1 x, $y + 1$, z; #2 x, y - 1, z.

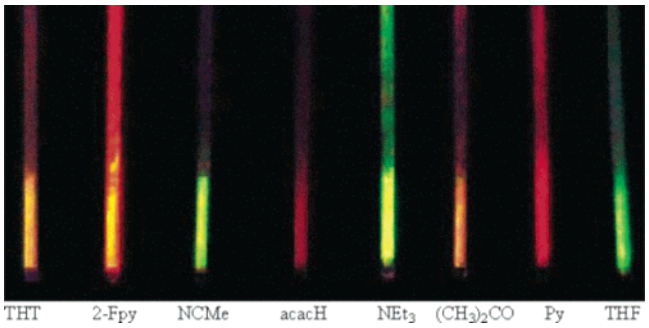

Figure 1. Powder samples of **1** deposited in glass tubes and exposed to selected organic vapors under UV light.

shows a butterfly cluster structure with the acetone ligand bridging the 2 Tl atoms instead of extended unsupported Au(I)···Tl(I) chains. Complexes **3**−**9** show characteristic colors: green for $\{Tl(THF)_2[Au(C_6Cl_5)_2]\}_n$, **3**; different yellow intensities for $\{Tl(THT)_2[Au(C_6Cl_5)_2]\}_n$, **4**, $\{Tl(2\text{-fluoropyridine})_2[Au(C_6Cl_5)_2]\}_n$, **6**, $\{Tl(NEt_3)_2[Au(C_6Cl_5)_2]\}_n$, **7**, and $\{Tl(NCMe)_2[Au(C_6Cl_5)_2]\}_n$, **9**; red for $\{Tl(acacH)_2[Au(C_6Cl_5)_2]\}_n$, **5**; and deep red for $\{Tl(py)_2[Au(C_6Cl_5)_2]\}_n$, **8**. All compounds are soluble in acetone and tetrahydrofuran and insoluble in dichloromethane and diethyl ether. The solutions of complexes **3**−**9** are stable in air and moisture for many hours without apparent decomposition, but they clearly undergo dissociation or chain degradation in solution.

The exposure of **1** in the solid state to VOCs has been studied and the results are shown in Figure 1. Exposure of **1** at RT to vapors of the volatile organic compounds employed as ligands for the synthesis of **2**−**9** leads to a perceptible change in the color of the solid. These colors, different for different organic ligands, revert to those of the starting materials upon heating the solid adducts to 100 °C for a few seconds in the case of THF to 10 min in the case of pyridine. In all complexes the process is completely reversible with no detectable degradation even after 10 exposure/heating cycles.

Table 3. Spectroscopic Data for Complexes **1**−**9**

	RT		77 K				
	exc (nm)	em (nm)	exc (nm)	em (nm)	lifetime (ns)	UV−vis (nm)[a]	IR (cm^{-1})
1	480	531	480	543	1000, 123	343	
2	422	556	420	556	2000, 700	500	1677[b]
3	417	479	421	489	2406, 315, 16	460	
4	500	560	479	560	262, 71, 9	467	
5	520	644	540	650	581, 153	530	1615, 1574[b]
6	410	599	420	610	1040, 2	430	1602[c]
7	498	554	470	559	443, 23, 12	459	
8	472	665	400	714	1143, 352	569	1590[c]
9	492	525	485	530	348, 91	453	2280[d]

[a] In solid state. [b] ν(C═O) stretching mode. [c] ν(C═N) stretching mode. [d] ν(C≡N) stretching mode.

^{1}H NMR Spectra. The ^{1}H NMR spectra of solutions of complexes **2**−**9** or VOCs derivatives display signals corresponding to the organic species (see Experimental Section). The chemical shifts are similar to those of the free organic ligands results expected due to dissociation in solution.

IR Spectra. The IR spectra **2**−**9** in Nujol mulls show absorptions arising from $C_6Cl_5^-$ groups in the ranges 836−839 and 612−616 cm^{-1}, corresponding to the ν(C−Cl) and ν(Au−C) modes, respectively.[11] In several complexes, where the Nujol oil and the polyethylene sheets do not mask the bands, absorptions due to the organic ligands coordinated to the Tl(I) centers can be assigned. They are at significantly different energies from absorptions for the uncoordinated organic ligands (see Table 3). For example, when complex **1** is exposed to acetone vapors the resulting product displays a band at 1677 cm^{-1} (1715 cm^{-1}, free ligand values in parentheses),[29] due to the ν(C═O) stretching vibration.

With acetylacetone the carbonyl stretches appear at 1615 and 1574 cm^{-1} (1622 cm^{-1}).[29] When the organic vapors are pyridine or 2-fluoropyridine the ν(C═N) stretch appears at 1509 (1581 cm^{-1}) and 1602 cm^{-1} (1581 and 1598 cm^{-1}), respectively.[29] Finally, in the acetonitrile derivative the ν(C≡N) stretch appears at 2280 cm^{-1} (2254 cm^{-1}).[29] In the rest of the samples (tetrahydrothiophene, tetrahydrofuran, or triethylamine) the characteristic absorptions are masked by other vibrational modes and assignments are not clear. In all cases the vibrational modes are shifted when compared with those of the free ligands. This is to be expected if there is an interaction of the donor atom of the ligand with the metal center. A comparison of the absorptions of the VOCs upon solid-state interactions with **1** with the spectra obtained for the isolated complexes **2**−**9** (see Tables 3 and 4) indicates a similar coordination of the VOCs to the thallium centers.

X-ray Crystal Structures. Structures of complexes **3** and **5** have been established by X-ray diffraction studies (Figures

(29) *SDBS Compound Information, www.aist.go.jp/RIODB/SDBS/menu-e.html.*

Table 4. Spectroscopic Data for Complex **1** Exposed to Different VOC Vapors

	RT		77 K			
VOC	exc (nm)	em (nm)	exc (nm)	em (nm)	UV−vis (nm)[a]	IR (cm^{-1})
none	480	531	480	543	343	
acetone	444	532	445	563	455	1677[b]
THF	473	507	472	530	482	
THT	485	567	491	604	489	
AcacH	550	650	547	681	539	1615, 1575[b]
2-fluoropyridine	400	627	391	660	455	1602[c]
NEt_3	463	511	487	539	460	
Py	560	646	595	757	600	1591[c]
NCMe	491	513	488	538	480	2282[d]

[a] In solid state. [b] ν(C═O) stretching mode. [c] ν(C═N) stretching mode. [d] ν(C≡N) stretching mode.

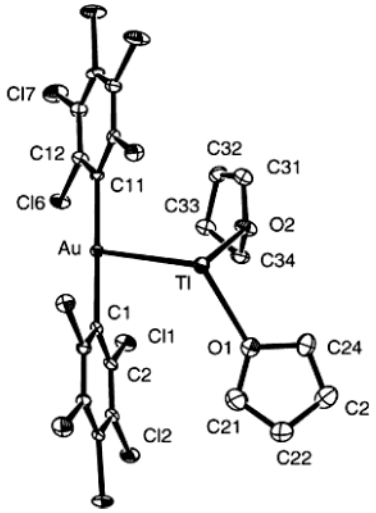

Figure 2. Asymmetric unit of complex **3**. Hydrogen atoms are omitted for clarity and ellipsoids are drawn at the 30% level.

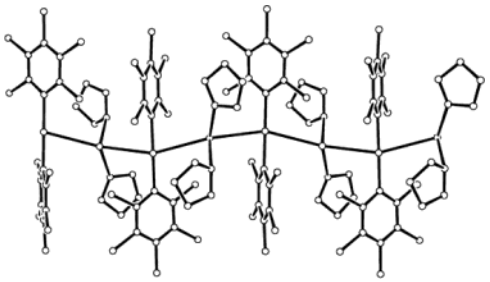

Figure 3. Polymeric crystal structure of **3**. Hydrogen atoms are omitted for clarity.

2−5 and Tables 1 and 2). In both cases the structures consist of polymeric chains formed by alternating $[Au(C_6Cl_5)_2]^-$ and $[TlL_2]^+$ (L = THF, **3**; acacH, **5**) units linked via short unsupported Au···Tl interactions of 3.0764(4) and 3.1981(4) Å, **3**, or 2.9684(5) and 2.9894(5) Å, **5**. These Au···Tl distances are close to the sum of thallium and metallic gold radii (3.034 Å). Each gold(I) center is linearly coordinated to two $C_6Cl_5^-$ ligands with Au−C distances of 2.071(8) and 2.082(8) Å for **3** or 2.063(10) and 2.069(9) Å for **5**. The thallium atoms show pseudo trigonal bipyramidal coordination with a vacant equatorial coordination site (presumably associated with a stereochemically active lone pair). The Tl−O distances in **3** (2.653(7) and 2.648(6) Å) and in **5**

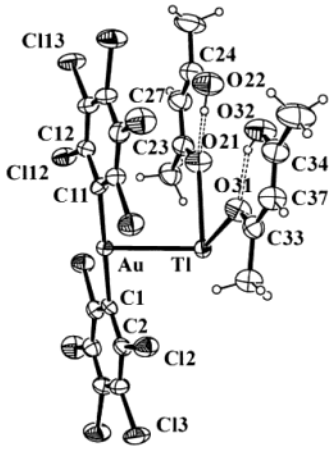

Figure 4. Asymmetric unit of **5**. Ellipsoids are drawn at the 30% level.

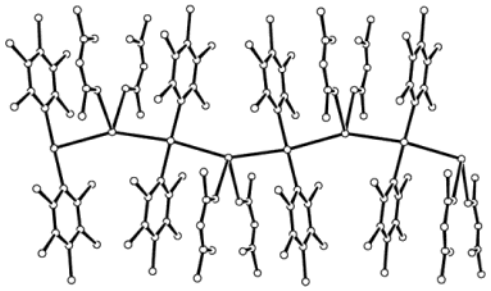

Figure 5. Polymeric crystal structure of **5**. Hydrogen atoms are omitted for clarity.

(2.626(8) and 2.692(9) Å) are shorter than the Tl−O (THF) distances observed in $[Tl(bipy)][Tl(bipy)_{0.5}(THF)][Au(C_6Cl_5)_2]_2$ (2.781(7) Å),[11] $[Au(C_6Cl_5)_2]_2[Tl(OPPh_3)][Tl(OPPh_3)(THF)]$ (2.766(5) Å),[10] or $[(THF)_2Tl(\mu\text{-NC})Mn(CO)(dppm)_2][PF_6]$ (2.74(3) and 2.75(3) Å),[30] or the Tl−O (acetone) distances observed in $[Au_2Tl_2(C_6Cl_5)_4]_2\cdot(CH_3)_2C{=}O$ (2.903(9) and 2.968(9) Å),[14] $[Au(C_6Cl_5)_2]_2[Tl(OPPh_3)][Tl(OPPh_3)(acetone)]$ (2.828(7) Å),[10] or $\{trans,trans,trans\text{-}[PtTl_2(C_6F_5)_2(C{\equiv}C^tBu)_2](acetone)_2\}_n$ (2.83(2) Å).[31] Each acetylacetone molecule in the crystal structure of **5** coordinates in its enol form, stabilized by an intramolecular O−H···O hydrogen bonding which gives rise to a six membered ring (Supporting Information). The Tl···Cl interactions between adjacent chains observed in the crystal structure[9] of **1**, which probably are responsible for its stability, are not present in **5**. A series of Au···Cl and Tl···Cl contacts between atoms of the same linear chain in the range 3.328(2)−3.790(2) for **3**, or 3.310(3)−3.729(3) Å for **5** are present and also may contribute to the stability of the systems.

Although attempts were made to obtain single crystals of the species resulting from treatment of solid **1** with VOCs, only in the case of THF were we able to separate X-ray quality crystals from the mixture of crystalline and noncrystalline species. These crystals were used for X-ray diffraction study which resulted in the structure shown in Figures 6 and 7. This structure is intermediate between the struc-

(30) Connelly, N. G.; Hicks, O. M.; Lewis, G. R.; Moreno, M. T.; Orpen, A. G. *J. Chem. Soc., Dalton Trans.* **1998**, 1913.
(31) Ara, I.; Berenguer, J. R.; Forniés, J.; Gómez, J.; Lalinde, E.; Merino, R. I. *Inorg. Chem.* **1997**, *36*, 6461.

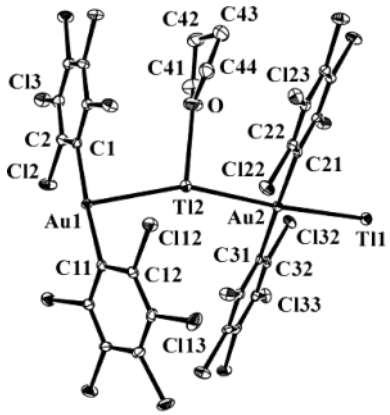

Figure 6. Asymmetric unit of **1** exposed to THF. Hydrogen atoms are omitted for clarity and ellipsoids are drawn at the 30% level.

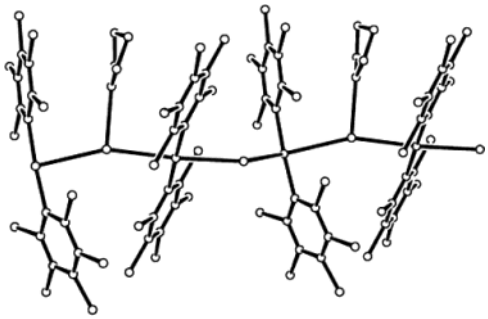

Figure 7. Polymeric crystal structure of **1**·0.5 THF, $\{Tl(THF)_{0.5}[Au(C_6Cl_5)_2]\}_n$. Hydrogen atoms are omitted for clarity.

ture of **1**,[9] in which there is no ligand coordinated to thallium, and complex **3**, which has two THF molecules per thallium. It consists of polymeric chains formed via unsupported Au···Tl interactions in the range 2.9078(3)−3.0918(3) Å, although in this case there is only one THF molecule per two thallium atoms. Thus, in the asymmetric unit, which contains four metal centers, instead of two as observed in **1**, **3**, and **5**, each thallium atom displays a different environment. While Tl(1) remains uncoordinated to THF with only intermetallic interactions and a Au−Tl−Au angle of 138.712(11)°, Tl(2) binds to the oxygen atom of a THF molecule. There is a nearly planar environment about Tl(2) with a sum of angles of 356.91° which is 0.2523(11) Å out of the plane defined by Au(1), Au(2), and O. The Tl−O distance of 2.697(6) Å is slightly longer than those observed in **3**, but also shorter than the Tl−O (THF) distances observed in other derivatives with Tl−O(THF) distances 2.74(3)−2.781(7) Å.[10,11,30] Finally, this structure also displays Au···Cl and Tl···Cl contacts between atoms of the same linear chain in the range 3.3211(17)−3.6437(18) Å, but also keeps some Tl···Cl interactions between adjacent chains in the range 3.2906(16)−3.5622(18) Å, as observed in the crystal structure of **1**.[9] These data also indicate that this structure is intermediate between those of **1** and **3**.

The absence of ligands coordinated to thallium in the crystal structure of **1** allows adjacent chains to get close to each other and to establish Tl···Cl interactions that give rise to vacant channels that run parallel to the crystallographic *z* axis (Figure 8a) with hole diameters as large as 10.471 Å, the shortest Au···Au distance between chains. These channels are large enough to accommodate the VOCs, which have been found to enter the lattice. When **1** is exposed to vapors of THF the organic molecules partially occupy these holes as observed in Figure 8b, but there are still vacant coordination sites at thallium and empty channels that might allow entrance of additional THF molecules. Finally, when the coordination sphere of each Tl(I) is complete with two THF molecules per thallium as observed in **3**, the Tl···Cl interactions between different chains are no longer present and the channels, which are now completely occupied, disappear (Figure 8c).

TGA Studies. TGA studies of complexes **2**−**9** show that none of them lose significant mass until decomposition. Thermogravimetric studies of the samples from the exposure of **1** to different donor vapors lose different amounts of donors per Tl(I) atom. As shown in Figure 9, the three samples presented here show different patterns of weight loss. After exposure of **1** to acetylacetone vapor, the TGA trace for the resulting product shows two steps: the first one at 58 °C in which the complex loses one mol of acetylacetone per Tl(I), and the second one at 102 °C in which the material loses 0.35 mol per Tl(I) atom. The temperatures at which the materials containing the VOCs lose the organic ligands are between 55 °C (THF) and 120 °C (acetone). The observed variations in the temperature of ligands loss are likely due to the different strengths of the interactions between the ligands and the thallium centers. None of these measurements show a loss corresponding to two moles of ligands per thallium. These studies further confirm that the absorption of organic VOCs by the solid complex **1** does not produce complete coordination of the thallium center, as observed for the complexes **2**−**9** prepared from solution reactions. These observations are in full accord with the assumption that the derivatives obtained from solid-phase exposure to the VOCs have compositions intermediate to the starting complex $\{Tl[Au(C_6Cl_5)_2]\}_n$, **1**, and those complexes obtained from the solution reactions, **2**−**9**.

Powder Diffraction Studies of the Vapochromic Materials. Several of the materials with VOCs obtained from the solid-phase reactions were studied by X-ray powder diffraction and compared with the data for the extended linear chain complex $\{Tl[Au(C_6Cl_5)_2]\}_n$, **1**, and calculated data from single-crystal structures. The powder pattern of **1**, collected between $2\theta = 5$ and $2\theta = 70°$, displays peaks with maxima at approximately $2\theta = 6$, 19, 33, 34, and 39° as shown in Figure 10a. These maxima match those of complex **1** obtained from single-crystal structure. Comparison of the powder diffraction pattern of **1** with those obtained for the materials containing the VOCs show substantial shifts and changes in intensity. A representative example, Figure 10, shows the change produced for **1** (Figure 10a) when it is exposed to 2-fluoropyridine vapor (Figure 10b), and after heating the sample in an oven at 100 °C for 10 min (Figure 10c). This latter Figure 10c shows a pattern indicative of complex **1** formed by loss of the VOC. At this point it is necessary to emphasize that the molecular complexes obtained from solution syntheses do not lose the organic

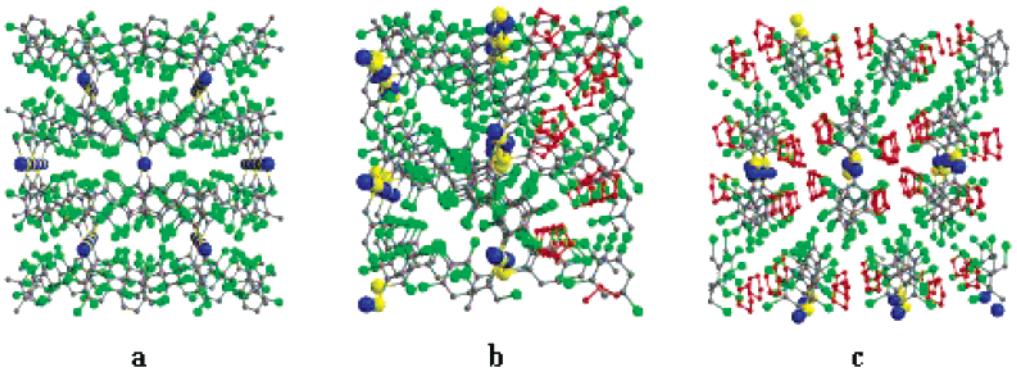

Figure 8. View of the crystal structure of complexes: (a) $\{Tl[Au(C_6Cl_5)_2]\}_n$, **1**; (b) **1** exposed to THF vapor; and (c) $\{Tl(THF)_2[Au(C_6Cl_5)_2]\}_n$, **3**. THF molecules are in red.

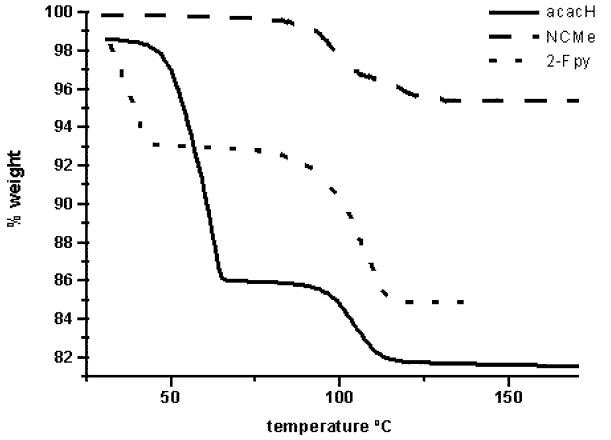

Figure 9. Thermogravimetric analyses showing the weight lost in several complexes.

Table 5. TDDFT RPA Singlet Excitation Calculations for the $\{Tl[Au(C_6Cl_5)_2]\}_2$ **1a** Model System

excitation	λcalc. (nm)	λexp. (nm)	oscil. str	contributions
A	547		0.16×10^{-1}	133a → 135a (55%) 132a → 135a (33%)
B	499	490	0.17	132a → 135a (63%) 133a → 135a (26%)
C	435		0.10×10^{-1}	128b → 135a
D	400	405	0.38×10^{-1}	131a → 135a (86%)
E	396		0.45×10^{-1}	127b → 135a (73%) 133a → 133b (9%)
F	383		0.301×10^{-1}	132a → 133b
G	357	355	0.126	128a → 135a (55%) 127a → 135a (18%)
H	347		0.38×10^{-1}	127a → 135a (59%) 127b → 132b (23%))
I	338		0.45×10^{-1}	126b → 132b

ligand bonded to Tl until decomposition. The X-ray powder diffraction analysis indicates that there is an appreciable change in the internal structure of **1** when it is exposed to different organic vapors which enter the lattice. Furthermore, this process is completely reversible upon heating, leading to regeneration of the starting material.

UV−vis Studies. Complexes **2**−**9** and the products from the exposure of **1** to VOCs show interesting optical properties. In addition to the absorption peaks at 217, 235, 288, and 311 nm for **1** in solution, which were assigned to the

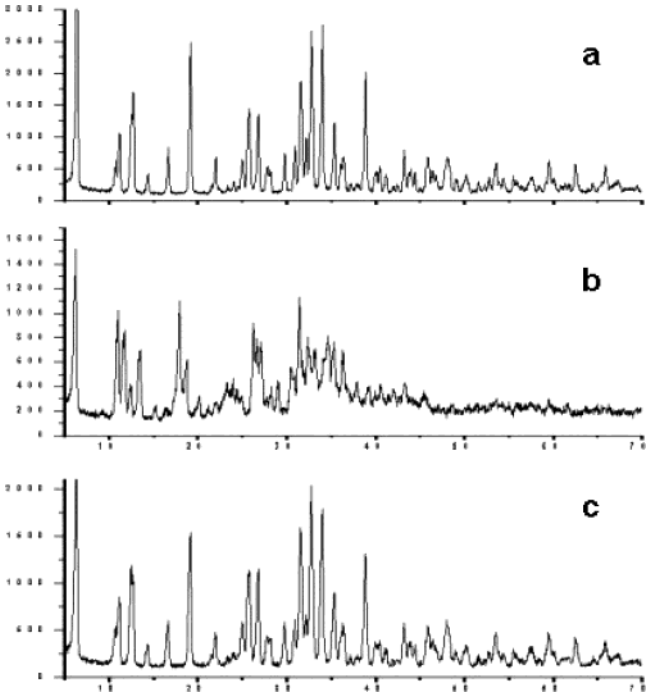

Figure 10. X-ray powder diffraction patterns for (a) $\{Tl[Au(C_6Cl_5)_2]\}_n$, **1**, (b) **1** exposed to 2-fluoropyridine vapor, and (c) after heating the sample in an oven at 100 °C for 10 min.

$[Au(C_6Cl_5)_2]^-$ units,[9] the UV−vis spectrum of **1** in the solid state shows an additional band with a maximum at 343 nm. This band has been assigned to a transition between levels formed as a consequence of the intermetallic Au(I)···Tl(I) interactions in the solid state.[9] This band also appears in the complexes **2**−**9**, but is significantly shifted to the red when compared to that of $\{Tl(NCMe)_2[Au(C_6Cl_5)_2]\}_n$, **9**, 453 nm, and $\{Tl(py)_2[Au(C_6Cl_5)_2]\}_n$, **8**, 569 nm (see Table 3). This suggests that this transition is associated with the presence of intermetallic Au(I)···Tl(I) interactions and is influenced by the coordination of ligands to the Tl(I) centers. It is known that the coordination of the organic ligands produces geometrical changes around each thallium center. These structural changes may lead to a change in the HOMO−LUMO band gap energy, and, hence, lower energy absorptions are observed.

For the UV−vis spectra of the species obtained from VOCs in solid state, the transition that appeared at 343 nm

in **1**, associated with the intermetallic interaction (see above), shifts to the visible region. New absorptions, from 455 nm, for acetone and 2-fluoropyridine, to 600 nm, for pyridine, are likely associated with the VOC-perturbed metal−metal interactions. As noted in Table 4, almost all of these absorptions appear at energies similar to the ones for complexes **2**−**9**. Weaker bands which appear as shoulders at high energy on the main bands are likely assigned to the interactions between gold and the coordinately unsaturated thallium centers, further supporting the fact that the thallium centers are not equally saturated in the structure.

Luminescence Studies. Luminescence measurements of complexes **2**−**9** and the materials obtained by the interactions of solid **1** with the VOCs show similar trends. Complexes **2**−**9** each display a strong visible luminescence over a wide range. The luminescence peaks occur (from high to low energy) at 479 (**3**, THF), 525 (**9**, NCMe), 554 (**7**, NEt_3), 556 (**2**, Me_2CO), 560 (**4**, THT), 599 (**6**, 2-fluoropyridine), 644 (**5**, acacH), and 665 (**8**, py). When **1** is exposed to vapor of these organic materials the change in color is even deeper under exposure to UV light and all the substances display a strong luminescence (see Figure 1). Exposure of **1** to the VOCs shifts the emission band from 531 nm at room temperature to 507 (THF), 511 (NEt_3), 513 (NCMe), 532 (Me_2CO), 567 (THT), 627 (2-fluoropyridine), 646 (py), and 650 nm (acacH), Table 4. When these latter emission spectra are compared with those obtained for complexes **2**−**9** (Table 3), the spectra are similar but with some subtle differences. These small differences can be attributed to differences in the compositions of **2**−**9** compared with the products obtained from the interactions of solid **1** with VOCs, as noted above. In all cases, the emission spectra are independent of the excitation wavelength.

The optical properties of the materials obtained by exposure of **1** to VOCs and the crystalline complexes **2**−**9** behave similarly with decreasing temperature. The emissions corresponding to both types of materials red shift at 77 K (see Tables 3 and 4). The observed shift of the emission to higher energies with increase in temperature is consistent with an increase in the metal−metal separation as a result of thermal expansion. This increased separation would increase the band gap energy. This suggests that the origin of the emission bands in these species (which depend on the extent of the metal−metal interactions) is similar to that proposed for **1**. This interaction also is influenced by the presence of the organic molecules in the lattice channels as in the case of the products from the solid **1** exposure to VOCs, or ligands coordinated to the Tl(I) centers as in **2**−**9**.

The absorptions attributed to the metal−metal interactions in the UV−visible spectra appear, in almost all cases, at energies similar to those in the excitation spectra. This strongly suggests that these transitions give rise to the observed luminescence. This supports the conclusion that the luminescence observed in these complexes has its origin largely in the gold−thallium interactions. Additionally, when the solids containing the VOCs or complexes **2**−**9** are dissolved in donor solvents they lose their emissions. This is likely due to the loss of the metal−metal interactions in solution. Evaporation of the solvents regenerates products with optical properties identical to those of the original materials.

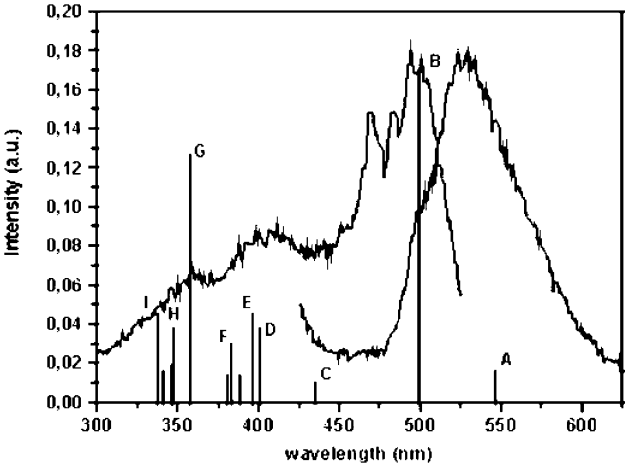

Figure 11. Excitation and emission spectra of compound **1** at room temperature in the solid state. Comparison between experimental excitation spectrum and theoretical oscillator strengths, *f*, from Table 5.

Theoretical Calculations. The interesting behavior of complex $\{Tl[Au(C_6Cl_5)_2]\}_n$, **1**, toward ligands, (i.e., VOCs) in solution or in the gas phase, and their photophysical properties prompted us to perform density functional theory (DFT) and time-dependent DFT (TDDFT) calculations. Single-point DFT calculations were performed first for the model dimer $\{[Au(C_6Cl_5)_2]\cdots Tl\cdots[Au(C_6Cl_5)_2]\cdots Tl\}$, **1a**, which was constructed from the X-ray diffraction results obtained for complex **1** assuming C_2 symmetry. A study of the MOs along with a population analysis was used to check the contribution of each atom to each occupied orbital (Supporting Information). Analyses of the highest energy occupied orbitals (133a, 132a, 128b, 131a, 127b, 126b, 128a, and 127a) shows that they are mainly centered on chlorine, carbon, and gold atoms. Therefore the HOMO orbitals are likely to be located on the $[Au(C_6Cl_5)_2]^-$ units. The 128a, 131a, 132a, and 133a orbitals also have contributions from the thallium atoms. For the lowest energy unoccupied orbitals, the populations cannot be analyzed, but their shapes can be checked. For each, the MOs are mainly located on the metal atoms. For instance, in 135a the four metal centers are involved, with a higher contribution of one of the thallium atoms (see Figure 12).

The TDDFT calculations allow us to predict excitations and to compare the energies and intensities with the experimental results (Figure 11). Thus, the singlet excitation energies of the model $\{[Au(C_6Cl_5)_2]\cdots Tl\cdots[Au(C_6Cl_5)_2]\cdots Tl\}$ **1a** were calculated at the TDDFT level (as described in the Computational Methods section). Only the singlet−singlet transitions were considered. Because one cannot estimate the strength of the spin−orbit effects on the singlet−triplet transitions, no singlet−triplet assignments have been made.

Table 5 lists the nine most intense energies for the model system and compares these results with the solid-state experimental excitation energies. Taking into account their oscillator strengths, the most important theoretical excitations are B and G. Excitation B gives a predicted energy of 499

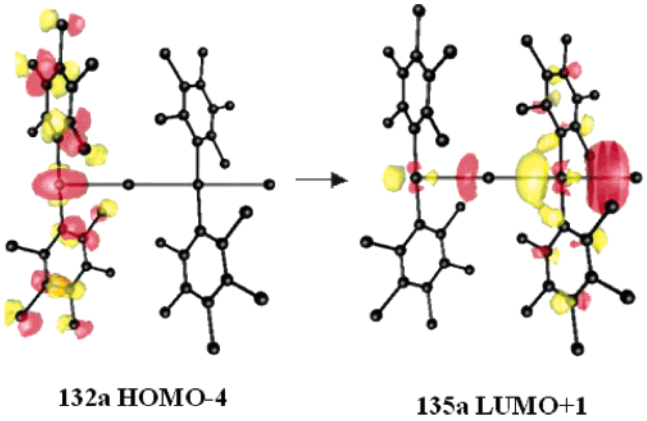

Figure 12. Orbitals involved in the main contribution to the B transition for the model compound $[TlAu(C_6Cl_5)_2]_2$, **1a**.

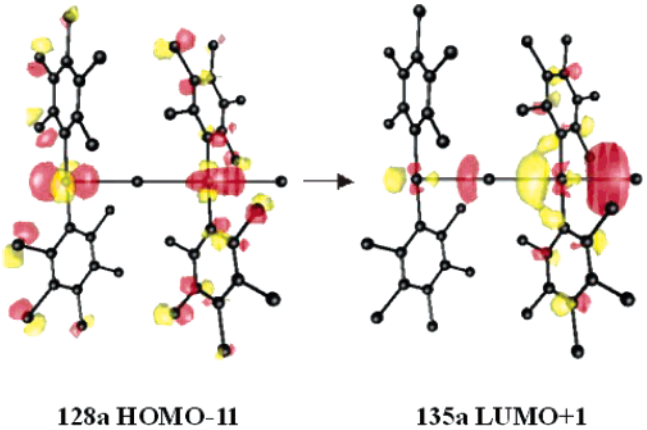

Figure 13. Orbitals involved in the main contribution to the G transition for the model $[TlAu(C_6Cl_5)_2]_2$, **1a** model system.

nm compared with the experimental excitation maximum at 490 nm. The most important contribution to this excitation then is the transition between the 132a (HOMO − 4) and 135a (LUMO + 1) orbitals (see Figure 12). Excitation G calculates energy of 355 nm which matches the experimental local maximum at 355 nm. Here the most important contribution is between 128a (HOMO − 11) and 135a (LUMO + 1) (Figure 13).

In the analyses of both the population of the higher energy occupied orbitals and the shapes of the lower energy virtual orbitals, it is reasonable to suggest that in the solid state there will be an excitation profile due to transitions arising from the basic $[Au(C_6Cl_5)_2]^-$ units to orbitals having a major contribution from the thallium atoms. The TDDFT calculations give theoretical excitation spectra that match with a very good accuracy the experimental results for complex **1**. As presented in Table 5, almost all these transitions have an acceptor orbital which is the metal based orbital 135a. This would indicate that the emission has most of its origin in this MO over all wavelengths excitation, as observed experimentally.

Finally, a detailed observation of the shape of the orbitals involved in the B and G transitions indicates electron transfer occurs between different atoms of the metallic chain. This is in accord with the excited-state being delocalized to some extent along the chain.

Summary

The extended unsupported linear chain complex $\{Tl[Au(C_6Cl_5)_2]\}_n$, **1**, reacts in solution with 2 equivalents of several organic ligands (L) to give extended, unsupported, crystalline zigzag-chain complexes of the type $\{TlL_2[Au(C_6Cl_5)_2]\}_n$, **3**−**9**. $\{Tl[Au(C_6Cl_5)_2]\}_n$ also is able to react in the solid state with volatile organic compounds, VOCs, to give new materials. In these materials the coordination of the ligands (or VOCs) takes place at the Tl(I) centers and gives rise to the new stoichiometric luminescent complexes **2**−**9** or materials containing a lower content of the VOCs. Although the type of coordination appears similar in both cases, as suggested by the IR spectra, the differences in the wavelengths in the UV−vis and the emission spectra can be explained in terms of different network structures. Thus, complexes **3**−**9** have complete ligation at the thallium centers, whereas complex **1**, when exposed to VOCs, does not fill all of the coordination sites of the Tl(I) centers.

TGA studies show that complex **1**, in the solid state, is able to absorb different amounts of VOCs, but always less than 2 equivalents per thallium atom as in **3**−**9**. The products resulting from the absorption of VOCs are assumed to be species with structures intermediate between complex **1** and complexes **3**−**9**. Indeed, the characterization of $\{Tl(THF)_{0.5}[Au(C_6Cl_5)_2]\}_n$ supports this idea. Moreover, as observed by powder X-ray diffraction, the products from solid-state reaction of **1** with the VOCs show a reversible loss of the VOCs by heating to 100 °C. The IR, TGA, and XRD data suggest that complex **1** can function as a reversible luminescent sensor for volatile organic species which coordinate to Tl(I) by diffusion into the channels created in this solid as a result of its 3D network of Au(I)···Tl(I) interactions.

Acknowledgment. The D.G.I. MCYT/FEDER (BQU2001-2409), CAR (ANGI2001/28), CSIC-Universidad de Chile (03/04-03), and the Robert A. Welch Foundation of Houston, Texas are acknowledged for financial support. M. M. thanks the MCyT-Universidad de La Rioja for his research contract "Ramón y Cajal".

Supporting Information Available: Tables of selected bond lengths and angles for **3**, **5**, and **1**·0.5 THF, hydrogen bonds for **5**, and population analysis for **1a**; and figures of exposed samples of **1** and UV-vis spectra for some different species (pdf). Crystallographic information files for the compounds studied (cif). This material is available free of charge via the Internet at http://pubs.acs.org.

IC0499446